

SCIENTIFIC REPORTS



OPEN

Assessment of Polysaccharides from Mycelia of genus *Ganoderma* by Mid-Infrared and Near-Infrared Spectroscopy

Yuhan Ma^{1,2,3}, Huaqi He^{1,2,3}, Jingzhu Wu⁴, Chunyang Wang^{1,2}, Kuanglin Chao⁵ & Qing Huang^{1,2} 

Ganoderma lingzhi (*G. lingzhi*), *G. sinense*, *G. applanatum*, etc. belongs to the *Ganoderma* genus of polypore mushrooms which contain rich polysaccharides valuable for nutrition and positive medicinal effects. In order to evaluate polysaccharide content in *Ganoderma* mycelia obtained in the fermentation process quickly and accurately, in this work we employed infrared spectroscopy to examine different *Ganoderma* stains of samples from diversified sources. Through mid-infrared (mid-IR) spectroscopy, we could identify the most relevant spectral bands required for polysaccharide evaluation, and through near-infrared (NIR) spectroscopy, we could establish the quantification model for making satisfactory prediction of polysaccharide ingredient content. As such, we have achieved an effective and convenient approach to quantitative assessment of the total polysaccharides in *Ganoderma* mycelia but also demonstrated that infrared spectroscopy can be a powerful tool for quality control of *Ganoderma* polysaccharides obtained from industrial production.

G. lingzhi, *G. sinense*, *G. applanatum*, etc. belongs to the genus *Ganoderma* which has been adopted as traditional Chinese herbal medicine in China since ancient times^{1,2}. Nowadays, researchers have proved that *G. lingzhi* and other *Ganoderma* species such as *G. sinense*, *G. applanatum*, etc. possess encouraging medical curing effects on hepatopathy, chronic hepatitis, nephritis, hypertension, arthritis, neurasthenia, insomnia, bronchitis, asthma, and gastric ulcers^{3,4}.

The major pharmacological ingredients of mushrooms in the *Ganoderma* genus include *Ganoderma* polysaccharides and ganoderic acids, and in particular, it has been reported that *Ganoderma* polysaccharides have some special functions such as therapeutic effects on cancer⁵⁻⁷, obesity^{8,9}, diabetes^{10,11}, and pancreatitis¹²; as well as pharmaceutical activity on immune modulation¹³⁻¹⁷, liver protection^{4,18,19}, and vascular endothelial cell growth inhibition^{20,21}. Especially, it has been reported that β -glucans in *Ganoderma* are closely related to health, for they can stimulate the immune response through cytotoxic or immunomodulatory mechanisms to enhance cellular immunity, and stimulate a variety of immune cells including macrophages²²⁻²⁴, neutrophils^{25,26}, natural killer cells^{27,28} and dendritic cells^{29,30}. In fact, *Ganoderma* polysaccharides extracted from mycelia and spores are used as prescription drugs in China by many pharmaceutical factories and companies.

Conventionally, polysaccharides can be examined through biochemical approaches such as the phenol-sulphuric acid method or anthrone-sulphuric acid method³¹. However, these methods normally require deleterious substances such as phenol, anthrone, and sulfuric acid³². In order to achieve a more convenient approach to quantitative assessment of polysaccharides in *Ganoderma mycelia*, non-destructive spectroscopic approaches including infrared spectroscopy thus become especially attractive for their outstanding advantages in cost, efficiency, sample preparation and instrument operation. In fact, infrared spectroscopy (including both mid-infrared

¹Key Laboratory of High Magnetic Field and Ion Beam Physical Biology, Institute of Technical Biology and Agriculture Engineering, Hefei Institutes of Physical Science, Chinese Academy of Sciences, Hefei, 230031, China. ²National Synchrotron Radiation Laboratory (NSRL), School of Life Science, University of Science and Technology of China (USTC), Hefei, 230026, China. ³College of Life Science, Anhui Science and Technology University, Fengyang, 233100, China. ⁴School of Computer and Information Engineering, Beijing Technology and Business University, Beijing, 100048, China. ⁵Environmental Microbial and Food Safety Laboratory, Agricultural Research Service, USDA, Beltsville, MD, 20705, USA. Correspondence and requests for materials should be addressed to Q.H. (email: huangq@ipp.ac.cn)

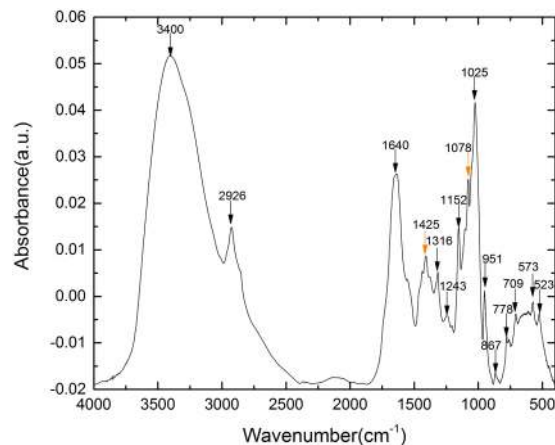


Figure 1. The mid-IR spectra of *G. lingzhi* mycelium dried powder.

and near-infrared spectroscopy) is widely used today in the agriculture^{33,34} and pharmaceutical industry^{35,36}, and shows great potential for the application in food processing industry as well^{37,38}.

In this context, therefore, we intended to employ infrared spectroscopy to assess polysaccharides in mycelia of different *Ganoderma* strains produced in the fermentation process. Although some previous studies have reported the application of both mid-IR- and NIR- spectroscopy in analysis of *Ganoderma* polysaccharides^{31,39}, there are still some problems yet to be solved for practical applications. For example, in the industrial production of *Ganoderma* polysaccharides, it is standard to produce *Ganoderma* mycelia through liquid fermentation, but there is neither a report for analysis of *Ganoderma* mycelia through mid-infrared (mid-IR) spectroscopy, nor a report of suitable near-infrared (NIR) quantification, that is valid for the assessment of polysaccharides in *Ganoderma* mycelia produced during the fermentation process. Therefore, in this work, we intended to combine both mid-IR and NIR techniques so that we could not only qualitatively analyze the samples based on mid-IR spectral data, but also quantitatively evaluate the polysaccharides in *Ganoderma* mycelia based on the optimized NIR quantification model.

Results

Analysis of *Ganoderma* mycelia via mid-IR spectroscopy. Mid-IR and NIR are both forms of electromagnetic radiation with wavelengths longer than visible light. The wavelength of mid-IR is between 4000–400 cm^{-1} (2.5–25 μm), while the wavelength of NIR with is between 14,000–4000 cm^{-1} (0.8–2.5 μm)⁴⁰. The absorption of mid-IR involves transitions between vibrational energy states and rotational sub-states of the molecule which can thus be employed for the elucidation molecular structure^{40,41}. A typical mid-IR spectrum of *G. lingzhi* mycelia is showed in Fig. 1, where the characteristic bands are shown with their assignments given in Table 1. The bands assigned to carbohydrates include the following: the bands at 1425 cm^{-1} ¹⁴², 1316 cm^{-1} ¹⁴³, 1152 cm^{-1} ¹⁴⁴, 1078 cm^{-1} ¹⁴⁵, 1025 cm^{-1} ^{146,47}, and 951 cm^{-1} ^{147,48}.

In addition, we also measured and analyzed different *Ganoderma* samples obtained in different stages during polysaccharide extraction process, with their mid-IR spectra shown in Fig. 2. From the spectrum, we can identify the characteristic bands attributed to carbohydrates, and we notice especially that the relative intensities of the bands at 1425 cm^{-1} and 1078 cm^{-1} are stronger for the samples with high content of polysaccharide after the extraction procedure.

Assessment of polysaccharide in *Ganoderma* mycelia by NIR spectroscopy. In addition, we employed the NIR spectroscopy for the quantification of the polysaccharide content in *Ganoderma* mycelia. Generally, NIR spectroscopy measures the broad overtone and combination bands of some of the fundamental vibrations and can be an excellent technique for rapid and quantitative evaluation of many chemicals⁴⁰. Figure 3a shows the NIR spectra in the 9000–4000 cm^{-1} region, and the corresponding first derivative spectra are shown in Fig. 3b. The absorption peaks at 8403 cm^{-1} , 6896 cm^{-1} , 5155 cm^{-1} are attributed to water⁴⁹, while the bands at 4307 cm^{-1} , 4405 cm^{-1} , 5787 cm^{-1} , and 5935 cm^{-1} are ascribed to carbohydrate. The NIR spectral band assignments are listed in Table 2.

To establish an optimal quantification model for polysaccharide assessment, we employed the methods of moving window partial least-squares (mwPLS) and interval PLS (iPLS) to find the appropriate spectral range for NIR quantification model. The mwPLS analysis (Figure S1a) shows that in the range of (5268.8–4000 cm^{-1}) the relative low root mean square error of cross validation (RMSECV) values are relatively low, and the iPLS analysis (Figure S1b) gives rise to the same consistent result. Accordingly, we took this range (5268.8–4000 cm^{-1}) and applied the constant offset elimination pre-treatment method for construction of the optimal quantification model. Our result shows that the optimal spectral range for *Ganoderma* mycelia is between 5268.8–4000 cm^{-1} , and the pre-treatment method is constant offset elimination (the comparisons using other different pre-treatment methods are given in the supplementary part Table S1). For the calibration set, we achieved determination coefficient (R^2) = 0.9779, RMSECV = 0.467, RPD = 6.73 at rank = 6, and for the prediction set we obtained root mean square error of prediction (RMSEP) = 0.603, relative percent deviation (RPD) = 3.13, correlation coefficient (corr.

Wavenumber(cm^{-1})	Functional Group Assignments
3400	-OH stretching ⁵⁵
2926	CH_2 asymmetric stretching ⁵⁶
1640	Amide I ⁵⁶
1457	CH_2 in polysaccharides ⁵⁷
1425	C-H deformation in lignin and carbohydrates ¹⁵
1372	C-H in-plane bending vibration ^{58,59}
1314–1316	symmetric CH_2 bending of cellulose ⁴³
1243	COH in-plane bending/CH in-plane bending ³⁸
1152–1156	C-O-C asymmetric stretching of glycosidic linkage ⁴⁴
1078	C-O stretching of β -glucans ^{45,46,51}
1044	stretching vibration of C-O-C group ⁶⁰
1025	stretching vibration of C-O α -glycosidic bond ⁴⁷
951	β -glycosidic bond ⁴⁷ ; C-O and C-C stretching ⁴⁸
867	γ (C-H) ⁶¹ ; furanose ring ⁶²
778	COO^- deformation ⁶³
709	CH out-of plane bending ⁶⁴
573	bending vibration of a polysaccharide ring ³⁹
523	pyranose ring ⁶² ; C=O asymmetric deformation ⁶⁵

Table 1. Assignments of the characteristic mid-IR bands in the mid-IR spectrum of *G. lingzhi mycelium*.

coeff.) = 0.9554. The calibration and prediction results are showed in Fig. 4. To check the model efficiency, the plot of RMSECV vs. Rank is also depicted and exhibits a smooth descent line (Figure S2).

Discussion

Qualitative analysis of *Ganoderma mycelia* based on mid-IR and NIR spectroscopy. In the foregoing sections, we have observed and identified the bands at 1425 cm^{-1} and 1078 cm^{-1} which are assigned to *Ganoderma* polysaccharides. These two bands are actually the most distinctive polysaccharide bands for our *Ganoderma mycelia* specimens. To confirm this, we measured the samples of high-content-polysaccharide (HCP) and low-content-polysaccharide (LCP) *G. lingzhi* strains, respectively, with the comparison of their mid-IR and NIR spectra as shown in Figs 5 and 6, respectively. We can see the prominent difference in intensity for the peaks at 1425 cm^{-1} and 1078 cm^{-1} , and correspondingly, we can also identify the most relevant polysaccharide bands in NIR spectra at 4307 cm^{-1} , 4405 cm^{-1} . These mid-IR and NIR bands are actually most useful for polysaccharide detection and quantification.

Furthermore, for the NIR analysis, we obtained the correlation coefficient curves based on the NIR spectra, and confirmed that the larger correlation coefficients also occur at these NIR spectral peak positions (Fig. 7).

These peaks are just assigned to polysaccharides (see the NIR band assignments listed in Table 1), and for this reason, our quantification model therefore covers the spectral range of $5268.8\text{--}4000 \text{ cm}^{-1}$ including the prominent bands at 4307 and 4405 cm^{-1} , which are closely related to their mid-IR counterparts, namely, the bands at 1425 cm^{-1} and 1078 cm^{-1} . These two mid-IR bands are actually corresponding to the C-H bending and C-O-H bending from pyranose ring of glucan, respectively, which exist widely in different kinds of mushrooms⁵⁰. More specifically, the characteristic mid-IR peak 1078 cm^{-1} is assigned to the C-O stretching in β -glucans of lignin and carbohydrates⁵¹, which is related with 4405 cm^{-1} in NIR spectra for it stems from O-H stretching and C-O stretching combination. The 1425 cm^{-1} peak corresponds to C-H deformation in lignin and carbohydrates⁴² and it is related with the 4307 cm^{-1} band in the NIR spectrum for it stems from C-H stretching and C-H₂ deformation combination. To further verify this, we also checked the relationship between the NIR spectra and the mid-IR spectra of *Ganoderma mycelia* based on a two-dimensional correlation spectroscopy of mid-IR and NIR spectra, as shown in Fig. 8. The result unambiguously confirms that the NIR range ($5268.8\text{--}4000 \text{ cm}^{-1}$) is most related to the mid-IR ($1422\text{--}1376 \text{ cm}^{-1}$) range which is mainly ascribed to polysaccharide in different *Ganoderma* stains.

To be noted, however, although quantification of total polysaccharide content is important for quality control of batch consistency, the total polysaccharide content is not necessarily correlated to health effect directly. As mentioned above, the medicinal value of *Ganoderma mycelium* is closely related to its β -glucans. Fortunately, one of the two selected peaks concerned in this work, namely the peak at 1078 cm^{-1} in FTIR (corresponding to NIR signal at 4405 cm^{-1}) is just the characteristic for β -glycosides. Therefore, while our NIR quantification model assisted by FTIR spectral analysis is valid for the assessment of total polysaccharide content, it may also be useful for a rough evaluation of β -glucans.

Comparison of our model with other quantification models. Considering the difference between mycelium and fruiting body of *Ganoderma* genus, it is understandable that our NIR quantification model is different from other previous models which contain broader spectral range. Although our NIR quantification model requires smaller spectral range, it actually gives rise to better prediction performance for providing larger range of polysaccharide values in the assessment.

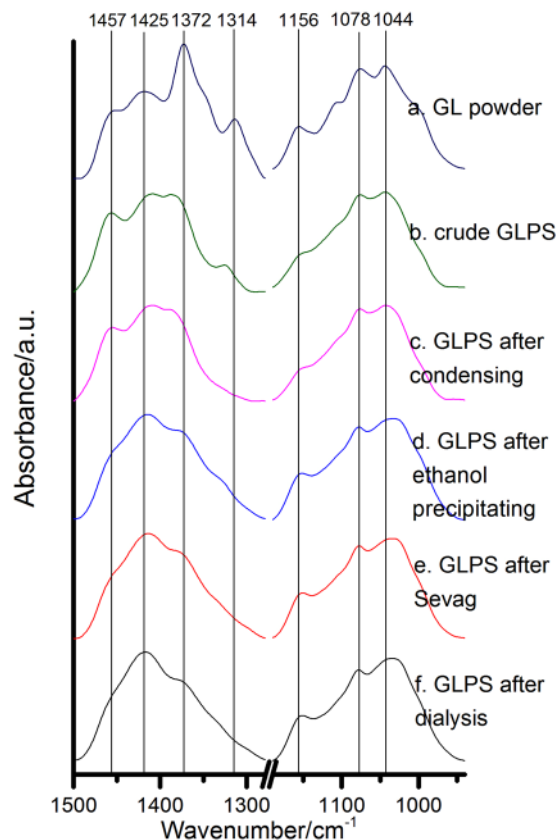


Figure 2. The mid-IR spectra of different samples obtained from the *G. lingzhi* polysaccharide extraction process. (a) GL powder refers to the drying powder from wet *G. lingzhi* culture mycelia; (b) crude GLPS refers to the extracted crude polysaccharide sample from the dried powder in 70 °C of hot water; (c) GLPS after condensing refers to the condensing supernatant sample using rotary vacuum approach; (d) GLPS after ethanol precipitating refers to the condensed remnant sample after ethanol precipitating process; (e) GLPS after Sevag refers to the sample with proteins removed with the by Sevag method; and (f) GLPS after dialysis refers to the sample which removed small molecular impurity substances after dialyzing process.

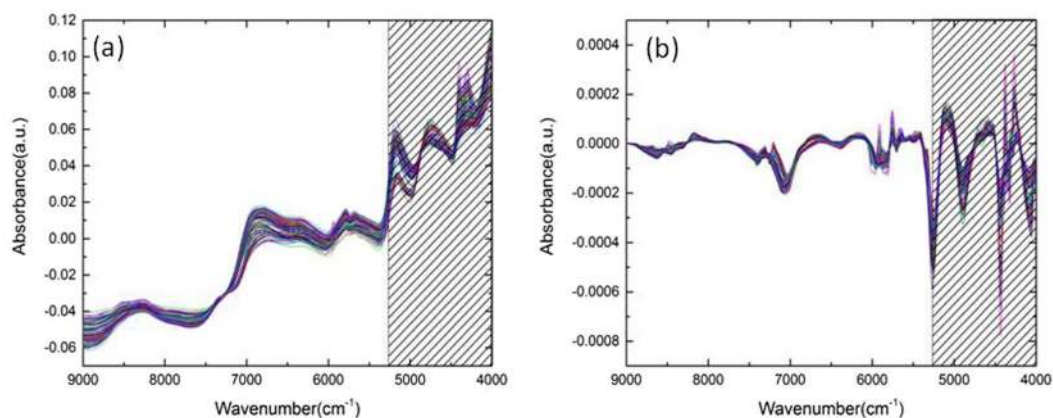


Figure 3. NIR spectra of *Ganoderma* mycelia with showing the selection of spectral range of 5268.8–4000 cm^{-1} for the optimal quantification assessment. (a) The conventional NIR spectra of *Ganoderma* mycelia; (b) The first derivative spectra of the corresponding NIR spectra.

It seems that it might be better to include bands such as 5787 and 5935 cm^{-1} bands in the quantification model as they also show relatively large correlation coefficients in Fig. 7. To check this, we chose the spectral range 6048–4000 cm^{-1} for comparison. The analysis of quantitative models for polysaccharides based on the NIR spectral range of (6048–4000 cm^{-1}) for calibration set and prediction set are shown in Figures S2 and S3. We noticed that it requires higher rank for the assessment (results listed in Table S2). Actually, when we just took the two bands at

Wavenumber (cm ⁻¹)	Type	Feature(s)
8403	combination of the first overtone of the O-H stretching and the OH-bending band (2ν _{1,3} + ν ₂)	Water ⁶⁶
6896	first overtone of the OH-stretching band (2ν _{1,3})	Water ⁶⁶
6674	first overtone of the OH-stretching band	alcohol or water ⁶⁶
6307	first overtone of the OH-stretching band	alcohol or water ⁶⁶
5935	C-H stretching first overtone	Lignin ⁶⁷ , hemicelluloses ^{67,68}
5787	C-H stretching (1st overtone) of -CH ₂	Carbohydrates ⁶⁹
5155	combination of stretching and deformation of the O-H group in water	Water ⁷⁰
4719	O-H and C-O stretching combination	Polysaccharide ⁷¹
4405	O-H stretching and C-O stretching combination	Polysaccharides ⁷²
4307	C-H stretching and C-H ₂ deformation combination	Polysaccharides ⁶⁶
4021	C-H stretching and C-C stretching combination	Cellulose ⁶⁶

Table 2. Assignments of the NIR absorption bands.

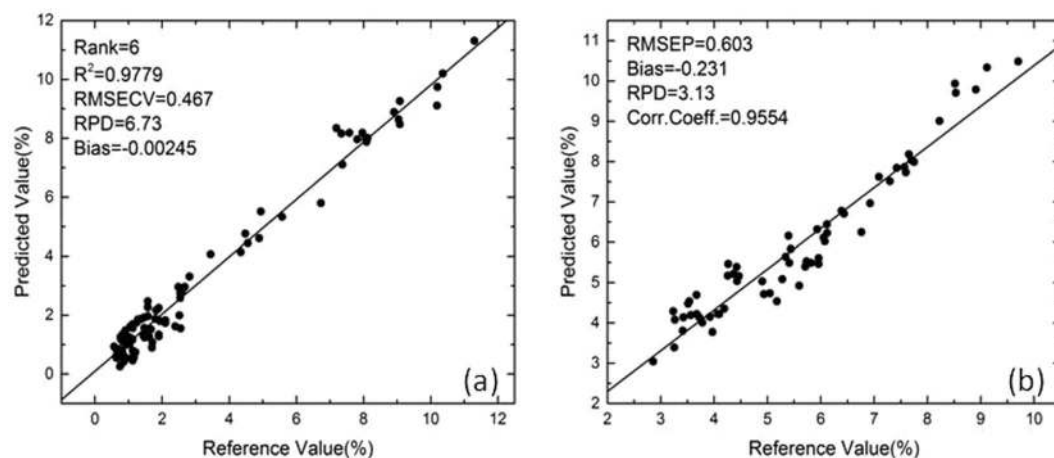


Figure 4. The NIR-based quantitative model for the polysaccharides on the range of (5268.8–4000 cm⁻¹) of calibration set (a) and prediction set (b).

4307 and 4405 cm⁻¹ in the construction of the quantification model, we obtained R² = 0.8505 and RPR = 2.59 for rank = 6 (Table S2). But if we took the other two bands at 5935 and 5787 cm⁻¹ into account, R² became smaller (R² = 0.8227) for rank = 6 (Table S2), with smaller RPD 2.37. So the efficiency or accuracy of the quantification model became worse. The reason may be understood with the following: First, we noticed that for the NIR spectra of *Ganoderma* fruiting body sample with high content of starch and cellulose, although the 4307 and 4405 cm⁻¹ bands are prominent in all the three spectra, the 5787 and 5935 cm⁻¹ bands are diminished in the spectra of cellulose and starch (Figure S4). Second, if we compare the spectrum of *Ganoderma* mycelium with that of *Ganoderma* fruiting body, we will find their NIR spectra are also really quite different (Figure S5). In *Ganoderma* fruiting body, the NIR signals are so weak for the 4307, 4405, 5787 and 5935 cm⁻¹ bands that they are almost invisible in the NIR spectra. Moreover, the spectral shapes are also very different. We explain that such a big difference in spectral features may be due to two factors. First, the compositional structure of mycelium and fruiting body is different. *Ganoderma* fruiting body has a very thick and hard crust consisting of high content of cellulose and lignin, whereas *Ganoderma* mycelium has neither cellulose nor lignin (or the contents of cellulose and lignin are almost negligible in *Ganoderma* mycelium). Second, the polysaccharide content between mycelia and fruiting bodies is also significantly different. As reported by Chen *et al.*³¹, the highest content of polysaccharides is about 8.07%. But in our mycelium samples, the content of polysaccharide is normally higher (up to 11.31%).

In summary, we have established an effective approach to polysaccharide content evaluation for *Ganoderma* mycelium samples, in which we utilized mid-infrared spectroscopy for qualitative analysis and NIR spectroscopy for quantitative assessment. The optimized model contains the region of (5268.8–4000 cm⁻¹) and with proper pre-treatment it can give rise to satisfactory prediction performance with the Rank = 6, R² = 0.9779, RMSECV = 0.467, RPD = 6.73 in the calibration set, and RMSEP = 0.603, RPD = 3.13, corr. coeff. = 0.9554 for the prediction set. This work therefore not only achieved an effective approach for establishment of a satisfactory quantification model for polysaccharide assessment in *Ganoderma* mycelia, but also set a good example of practical application of NIR spectroscopy in the assessment of *Ganoderma* polysaccharides in industrial production.

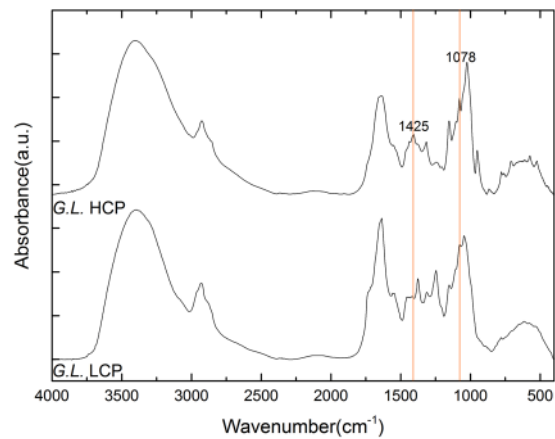


Figure 5. The mid-IR spectra of HCP and LCP *G. lingzhi* mycelia. HCP: high content of polysaccharide; LCP: low content of polysaccharide.

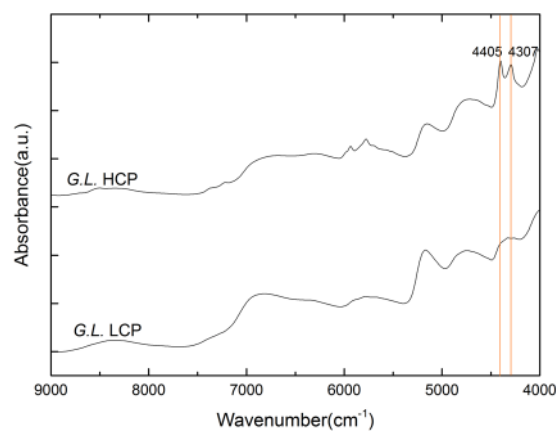


Figure 6. The NIR spectra of both HCP and LCP *G. lingzhi* mycelia, showing the most critical characteristic bands for assessment of polysaccharides.

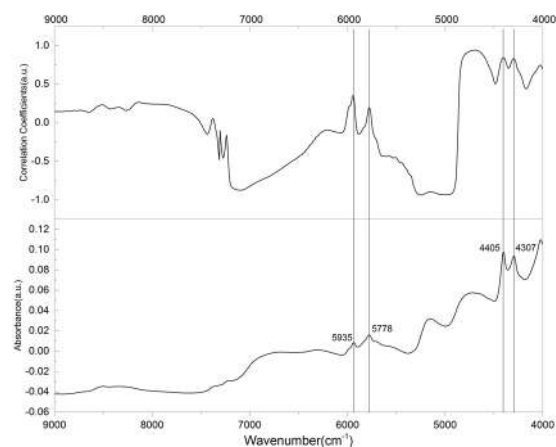


Figure 7. Correlation coefficients of the chemical measurements with the comparison with NIR spectra.

Methods

Materials. The *G. lingzhi* strain 5.0026 was purchased from China General Microbiological Culture Collection Center (CGMCC), while some other *Ganoderma* strains were collected in 10 different provinces in China including Anhui, Shandong and Sichuan, etc.

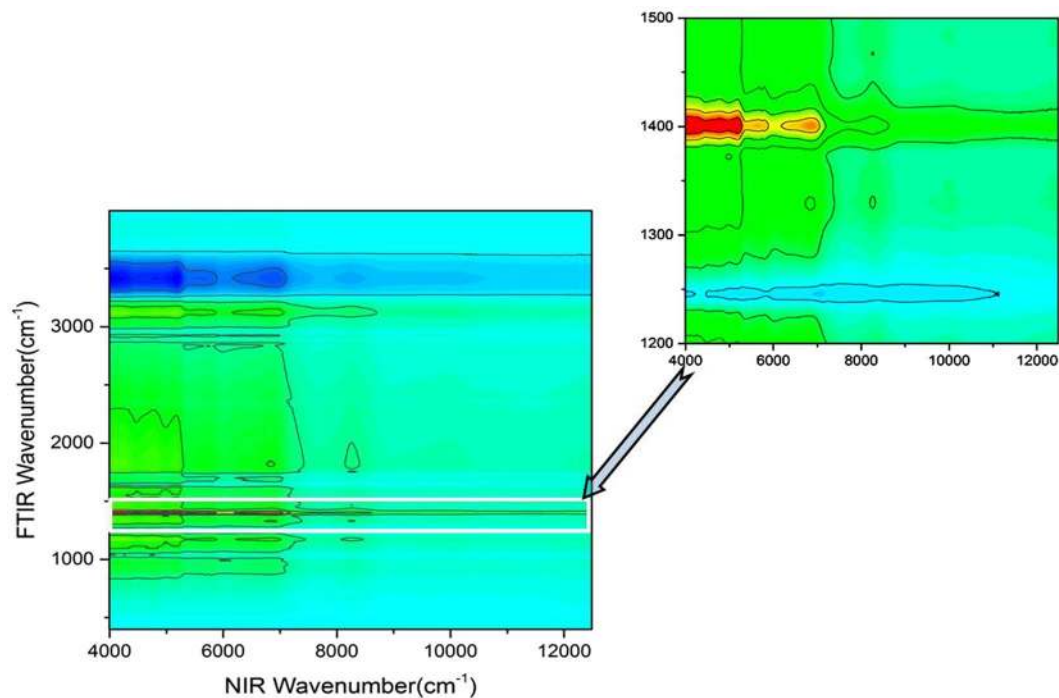


Figure 8. Correlation spectroscopy of NIR and mid-IR spectra of *Ganoderma* mycelia, showing that the NIR spectral range (5268–4000 cm^{-1}) is most related to the mid-IR spectral range (1422–1376 cm^{-1}).

In order to make the range of the experimental samples with polysaccharide contents wide enough, 51 *in vitro* axenic preservation *Ganoderma* strains were purchased, exchanged or isolated from wild fruiting bodies. Among them, 38 strains were *G. lingzhi*, 7 strains were *G. applanatum*, 3 strains were *G. sinense*, 2 strains were *G. resinaceum*, and 1 strain was *G. leucocontextum*. Taking into account of the changes in polysaccharide content of mycelia at different fermentation stages, each strain was cultured for 7 days, 14 days and 21 days, respectively. On the 7th day, most mycelia were in the logarithmic growth phase, and they grew very fast; on the 14th day, most culture flasks were filled with mycelia; on the 21st day, all flasks were full of mycelia, and a few strains started to form its fruiting body. All the 153 mycelium samples were washed with ddH₂O for three times, placed into petri dishes at -60°C for 48 hours to freeze for drying (FD-1D-50, Bilon, China). All these strains were randomly selected into calibration (90 samples) and validation sets (63 samples).

All the *Ganoderma* strains were activated in PDA solid medium and then transferred into Potato Dextrose Broth for 7 days, 14 days and 21 days, respectively. For the mid-IR measurements, the mycelia were lyophilized and pulverized into powders for future testing.

Sample grouping and polysaccharide contents (reference and predicted value) were shown in the Table S3. Many of the mycelia were morphologically different in terms of size, color, and viscous degree of the culture solution with some samples demonstrated in Figure S6.

Extraction and purification of *Ganoderma* polysaccharides. 140 g fermented *Ganoderma* mycelia dried powder, with adding 7 L ddH₂O, was placed into 70°C hot water bath for 2 hours for the polysaccharide extraction. The extract liquid was then taken into centrifuge tubes, centrifuged at 4400 rcf/g for 10 min (3K15, Sigma Laborzentrifugen, Germany), kept at 20°C for 15 min, and then the mycelia precipitate was separated from the crude water-soluble polysaccharide supernatant. The supernatant was then concentrated in a rotary evaporator under reduced pressure at 60°C to get 850 ml of vacuum-concentrated liquid. The concentrated extract solution was precipitated with 3.4 L ethanol and kept at 4°C overnight. The precipitate was obtained by centrifugation at 4400 rcf/g for 15 min, and then dried at 45°C for 2 hours, giving the crude polysaccharides. The crude polysaccharide was then re-dissolved with 800 ml ddH₂O. 500 ml of the re-dissolved polysaccharide was treated with Sevag reagent (1:4 n-butanol: chloroform, v/v, 120 ml) to remove the proteins inside the solution³⁹. The mixture was violently oscillated for 30 min and centrifuged to remove the denatured proteins at the interface between water layer and Sevag reagent layer. The above operation was repeated until no denatured proteins appeared. In order to decolor the solution, 1.5% (v/v) activated charcoal was added to the Sevag-treated crude polysaccharide, with thermostatic water bathing for 40 minutes, then the polysaccharide solution was poured into a dialysis bag, with both ends tightened up, and placed into ddH₂O. The water was changed every 4 hours, until the color of the dialysate did not change.

Preparation of freeze-dried polysaccharide samples from *Ganoderma* genus. Each liquid sample obtained from the steps mentioned above was pipetted and placed into petri dishes at -60°C for 48 hours to freeze for drying (FD-1D-50, Bilon, China). So we obtained the following samples: a. The GL powder means the drying powder from wet *Ganoderma* culture mycelia. b. The crude GLPS means the extracted crude polysaccharide from

the dried powder in 70 °C of hot water. c. The GLPS after condensing is the condensing supernatant using rotary vacuum approach. d. The GLPS after ethanol precipitating means the condensed remnant after ethanol precipitating process. e. The GLPS after Sevag means the polysaccharides removing proteins with the by Sevag method. f. The GLPS after dialysis means the polysaccharide samples which remove small molecular impurity substances after dialyzing operation. These samples were then examined by infrared spectroscopy.

Measurement of polysaccharides in dried mycelia of different Ganoderma stains. 2 ml of 0.012, 0.024, 0.036, 0.048, 0.06, 0.072, and 0.084 mg/ml glucose solutions were prepared, respectively. Then, 6 ml of anthrone reagent was added to each glucose solution and the solution was first kept at room temperature for 15 minutes, and then stored on ice for 15 minutes. When the test tubes were cooled and 3 ml of each sample was read at 625 nm wavelength using UV–vis spectrophotometer (Shimadzu UV-2550, Japan). The spectrum value at 625 nm was recorded for analysis. A standard curve for total carbohydrate assay was generated. The determination coefficient (R^2) of glucose standard curve is 0.9903, with the standard error less than 0.001⁵².

0.1 g of the lyophilised sample was mixed with 10 ml ddH₂O, and placed steady for 1 h. After that, the mixture was placed in 70 °C hot water bath for 2 hours, centrifugated after cooling, and the precipitate was discarded. The supernatant was diluted 20 times and 2 ml sample solution was pipette into a test tube for measurement. 6 ml sulfuric acid solution was added into the test tube and mixed with the sample together. The mixed sample was measured at 625 nm using the UV–Vis spectrophotometer. The content of polysaccharide was then calculated referring to standard curve above (g glucose/100 g sample). And the Ganoderma polysaccharide content was used as reference value for the quantification model⁵².

Measurements of mid-IR spectra. The samples for mid-IR measurement were prepared by mixing 2 mg of freeze-dried *Ganoderma* mycelia samples with 200 mg of dried potassium bromide followed by pressing under pressure 15 MPa for 3 minutes to make a disk pellet. The samples were then subjected to mid-IR measurements, and the spectral range (4000–400 cm⁻¹) was recorded using a Bruker ALPHA-T instrument (Bruker Optics GmbH, Ettlingen, Germany) with a resolution of 4 cm⁻¹ and 64 scans per sample. The results were then analyzed using OPUS 7.0 data processing software.

Measurement of NIR spectra. A FT-NIR spectrometer (NIR MPA, Bruker Optik GmbH, Germany) was used to collect the diffuse reflection spectra, with a resolution of 16 cm⁻¹ and 32 scans per sample ranged from 12500–4000 cm⁻¹. Each sample was tested several times for the average. These results were then analyzed by OPUS 7.0 data processing software.

Data analysis. Both NIR and mid-IR spectral data were analyzed using OPUS software (Bruker Optik GmbH, Ettlingen, Germany). Before the spectral data analysis, all the spectra were pre-treated using the procedures of vector normalization and baseline correction. After the spectra were collected, the spectra were exported from OPUS software and imported directly into program IBM SPSS Statistics 19 (SPSS) for cluster analysis, and OriginPro 2016 software (OriginLab Corporation, Northampton, Massachusetts, USA.) for figure graphing.

The data analysis methods including moving window partial least squares (mwPLS), interval partial least squares (iPLS) and correlation coefficient were conducted using iToolbox (programmed by Prof. L. Nørgaard, KVL, Denmark, published on <http://www.models.kvl.dk/iToolbox>) on Matlab2012b^{53,54}. Both mwPLS and iPLS are the efficient algorithms used to optimize the spectral range for a quantification model: mwPLS builds a series of PLS models in a window that moves over the whole spectral region and then locates useful spectral intervals in terms of the least complexity of PLS models reaching a desired error level^{53,54}, while iPLS is an interactive extension to PLS which develops local PLS models on equidistant subintervals of the full-spectrum region and focuses on important spectral regions and removing interferences from other regions⁵⁰.

References

- Paterson, R. R. M. & Lima, N. Editorial for the special issue on Ganoderma. *Phytochemistry* **114**, 5–6, <https://doi.org/10.1016/j.phytochem.2015.04.008> (2015).
- Zhou, L. W. *et al.* Global diversity of the Ganoderma lucidum complex (Ganodermataceae, Polyporales) inferred from morphology and multilocus phylogeny. *Phytochemistry* **114**, 7–15, <https://doi.org/10.1016/j.phytochem.2014.09.023> (2015).
- Paterson, R. R. Ganoderma - a therapeutic fungal biofactory. *Phytochemistry* **67**, 1985–2001, <https://doi.org/10.1016/j.phytochem.2006.07.004> (2006).
- Zhu, K. X. *et al.* A Polysaccharide from Ganoderma atrum Improves Liver Function in Type 2 Diabetic Rats via Antioxidant Action and Short-Chain Fatty Acids Excretion. *J Agric Food Chem* **64**, 1938–1944, <https://doi.org/10.1021/acs.jafc.5b06103> (2016).
- Jiang, D. *et al.* Restoration of the tumor-suppressor function to mutant p53 by Ganoderma lucidum polysaccharides in colorectal cancer cells. *Oncology Reports* **37**, 594–600, <https://doi.org/10.3892/or.2016.5246> (2017).
- Chan, K. M. *et al.* Screening and analysis of potential anti-tumor components from the stipe of Ganoderma sinense using high-performance liquid chromatography/time-of-flight mass spectrometry with multivariate statistical tool. *Journal of Chromatography A* **1487**, 162–167, <https://doi.org/10.1016/j.chroma.2017.01.044> (2017).
- Li, W. J. *et al.* Enhancement of Cyclophosphamide-Induced Antitumor Effect by a Novel Polysaccharide from Ganoderma atrum in Sarcoma 180-Bearing Mice. *Journal of Agricultural and Food Chemistry* **59**, 3707–3716, <https://doi.org/10.1021/jf1049497> (2011).
- Chang, C. J. *et al.* Ganoderma lucidum reduces obesity in mice by modulating the composition of the gut microbiota. *Nature Communications* **6**, <https://doi.org/10.1038/ncomms8489> (2015).
- Delzenne, N. M. & Bindels, L. B. GUT MICROBIOTA Ganoderma lucidum, a new prebiotic agent to treat obesity? *Nature Reviews Gastroenterology & Hepatology* **12**, 553–554, <https://doi.org/10.1038/nrgastro.2015.137> (2015).
- Xiao, C. *et al.* Antidiabetic activity of Ganoderma lucidum polysaccharides F31 down-regulated hepatic glucose regulatory enzymes in diabetic mice. *Journal of Ethnopharmacology* **196**, 47–57, <https://doi.org/10.1016/j.jep.2016.11.044> (2017).
- Jung, S. H. *et al.* Inhibitory effects of Ganoderma applanatum on rat lens aldose reductase and sorbitol accumulation in streptozotocin-induced diabetic rat tissues. *Phytotherapy Research* **19**, 477–480, <https://doi.org/10.1002/ptr.1638> (2005).
- Li, K. K. *et al.* Three kinds of Ganoderma lucidum polysaccharides attenuate DDC-induced chronic pancreatitis in mice. *Chemico-Biological Interactions* **247**, 30–38, <https://doi.org/10.1016/j.cbi.2016.01.013> (2016).

13. Zhang, J. J., Gao, X., Pan, Y. G., Xu, N. & Jia, L. Toxicology and immunology of Ganoderma lucidum polysaccharides in Kunming mice and Wistar rats. *International Journal of Biological Macromolecules* **85**, 302–310, <https://doi.org/10.1016/j.ijbiomac.2015.12.090> (2016).
14. Zhao, H. Y. *et al.* Enteric Mucosal Immune Response might Trigger the Immunomodulation Activity of Ganoderma lucidum Polysaccharide in Mice. *Planta Medica* **76**, 223–227, <https://doi.org/10.1055/s-0029-1186055> (2010).
15. Zhu, X. L., Chen, A. F. & Lin, Z. B. Ganoderma lucidum polysaccharides enhance the function of immunological effector cells in immunosuppressed mice. *Journal of Ethnopharmacology* **111**, 219–226, <https://doi.org/10.1016/j.jep.2006.11.013> (2007).
16. Yue, G. G. L. *et al.* Immunomodulatory Activities of Ganoderma sinense Polysaccharides in Human Immune Cells. *Nutrition and Cancer-an International Journal* **65**, 765–774, <https://doi.org/10.1080/01635581.2013.788725> (2013).
17. Manayi, A., Vazirian, M., Zade, F. H. & Tehranifard, A. Immunomodulation Effect of Aqueous Extract of the Artist's Conk Medicinal Mushroom, Ganoderma applanatum (Agaricomycetes), on the Rainbow Trout (*Oncorhynchus mykiss*). *International Journal of Medicinal Mushrooms* **18**, 927–933 (2016).
18. Wang, X. *et al.* Effects of Ganoderma lucidum polysaccharide on CYP2E1, CYP1A2 and CYP3A activities in BCG-immune hepatic injury in rats. *Biological & Pharmaceutical Bulletin* **30**, 1702–1706, <https://doi.org/10.1248/bpb.30.1702> (2007).
19. Liu, Y. J. *et al.* Anti-inflammatory and hepatoprotective effects of Ganoderma lucidum polysaccharides on carbon tetrachloride-induced hepatocyte damage in common carp (*Cyprinus carpio* L.). *International Immunopharmacology* **25**, 112–120, <https://doi.org/10.1016/j.intimp.2015.01.023> (2015).
20. Wang, S. H. *et al.* Ganoderma lucidum polysaccharides prevent platelet-derived growth factor-stimulated smooth muscle cell proliferation *in vitro* and neointimal hyperplasia in the endothelial-denuded artery *in vivo*. *Journal of Cellular Physiology* **227**, 3063–3071, <https://doi.org/10.1002/jcp.23053> (2012).
21. Cao, Q. Z. & Lin, Z. B. Ganoderma lucidum polysaccharides peptide inhibits the growth of vascular endothelial cell and the induction of VEGF in human lung cancer cell. *Life Sciences* **78**, 1457–1463, <https://doi.org/10.1016/j.lfs.2005.07.017> (2006).
22. Chan, G. C. F., Chan, W. K. & Sze, D. M. Y. The effects of beta-glucan on human immune and cancer cells. *Journal of Hematology & Oncology* **2**, <https://doi.org/10.1186/1756-8722-2-25> (2009).
23. Wang, C. H. *et al.* Concentration Variation and Molecular Characteristics of Soluble (1,3;1,6)-beta-D-Glucans in Submerged Cultivation Products of Ganoderma lucidum Mycelium. *Journal of Agricultural and Food Chemistry* **62**, 634–641, <https://doi.org/10.1021/jf404533b> (2014).
24. Javed, S., Payne, G. W. & Lee, C. H. Ganoderma applanatum - potential target for stimulating macrophages in immunosuppressive breast cancer microenvironment. *Breast Cancer Research and Treatment* **159**, 181–181 (2016).
25. Hsu, M. J., Lee, S. S. & Lin, W. W. Polysaccharide purified from Ganoderma lucidum inhibits spontaneous and Fas-mediated apoptosis in human neutrophils through activation of the phosphatidylinositol 3 kinase/Akt signaling pathway. *Journal of Leukocyte Biology* **72**, 207–216 (2002).
26. Hsu, M. J., Lee, S. S., Lee, S. T. & Lin, W. W. Signaling mechanisms of enhanced neutrophil phagocytosis and chemotaxis by the polysaccharide purified from Ganoderma lucidum. *British Journal of Pharmacology* **139**, 289–298, <https://doi.org/10.1038/sj.bjp.0705243> (2003).
27. Wu, Y. S., Ho, S. Y., Nan, F. H. & Chen, S. N. Ganoderma lucidum beta 1,3/1,6 glucan as an immunomodulator in inflammation induced by a high-cholesterol diet. *Bmc Complementary and Alternative Medicine* **16**, <https://doi.org/10.1186/s12906-016-1476-3> (2016).
28. Chen, S. N. *et al.* The Effect of Mushroom Beta-Glucans from Solid Culture of Ganoderma lucidum on Inhibition of the Primary Tumor Metastasis. *Evidence-Based Complementary and Alternative Medicine*, <https://doi.org/10.1155/2014/252171> (2014).
29. Yoshida, H. *et al.* Preferential induction of Th17 cells *in vitro* and *in vivo* by Fucogalactan from Ganoderma lucidum (Reishi). *Biochemical and Biophysical Research Communications* **422**, 174–180, <https://doi.org/10.1016/j.bbrc.2012.04.135> (2012).
30. Han, X. Q. *et al.* Structure Elucidation and Immunomodulatory Activity of A Beta Glucan from the Fruiting Bodies of Ganoderma Sinense. *Plos One* **9**, <https://doi.org/10.1371/journal.pone.0100380> (2014).
31. Chen, Y. *et al.* Quantification of total polysaccharides and triterpenoids in Ganoderma lucidum and Ganoderma atrum by near infrared spectroscopy and chemometrics. *Food Chemistry* **135**, 268–275, <https://doi.org/10.1016/j.foodchem.2012.04.089> (2012).
32. Kume, S. *et al.* Relationships between crude protein and mineral concentrations in alfalfa and value of alfalfa silage as a mineral source for periparturient cows. *Animal Feed Science and Technology* **93**, 157–168, [https://doi.org/10.1016/s0377-8401\(01\)00281-4](https://doi.org/10.1016/s0377-8401(01)00281-4) (2001).
33. Tinti, A., Tugnoli, V., Bonora, S. & Francioso, O. Recent applications of vibrational mid-Infrared (IR) spectroscopy for studying soil components: a review. *Journal of Central European Agriculture* **16**, <https://doi.org/10.5513/jcea.v16i1.3483> (2015).
34. Siesler, H. W., Ozaki, Y., Kawata, S. & Heise, H. M. *Near-infrared spectroscopy - Principles, instruments, applications*. (Wiley-Vch, Inc, 2002).
35. Guo, T. *et al.* Fourier transform mid-infrared spectroscopy (FT-MIR) combined with chemometrics for quantitative analysis of dextrin in Danshen (*Salvia miltiorrhiza*) granule. *J Pharm Biomed Anal* **123**, 16–23, <https://doi.org/10.1016/j.jpba.2015.11.021> (2016).
36. Jamrogiewicz, M. Application of the near-infrared spectroscopy in the pharmaceutical technology. *J Pharm Biomed Anal* **66**, 1–10, <https://doi.org/10.1016/j.jpba.2012.03.009> (2012).
37. Teixeira dos Santos, C. A., Lopo, M., Pascoa, R. N. M. J. & Lopes, J. A. A Review on the Applications of Portable Near-Infrared Spectrometers in the Agro-Food Industry. *Applied Spectroscopy* **67**, 1215–1233, <https://doi.org/10.1366/13-07228> (2013).
38. Hell, J. *et al.* A comparison between near-infrared (NIR) and mid-infrared (ATR-FTIR) spectroscopy for the multivariate determination of compositional properties in wheat bran samples. *Food Control* **60**, 365–369, <https://doi.org/10.1016/j.foodcont.2015.08.003> (2016).
39. Choong, Y. K. *et al.* Determination of storage stability of the crude extracts of Ganoderma lucidum using FTIR and 2D-IR spectroscopy. *Vibrational Spectroscopy* **57**, 87–96, <https://doi.org/10.1016/j.vibspec.2011.05.008> (2011).
40. Larkin, P. *Infrared and Raman spectroscopy: principles and spectral interpretation*. (Elsevier, 2011).
41. Kacurakova, M. & Wilson, R. H. Developments in mid-infrared FT-IR spectroscopy of selected carbohydrates. *Carbohydrate Polymers* **44**, 291–303, [https://doi.org/10.1016/s0144-8617\(00\)00245-9](https://doi.org/10.1016/s0144-8617(00)00245-9) (2001).
42. Naumann, A., Navarro-Gonzalez, M., Peddireddi, S., Kues, U. & Polle, A. Fourier transform infrared microscopy and imaging: detection of fungi in wood. *Fungal Genet Biol* **42**, 829–835, <https://doi.org/10.1016/j.fgb.2005.06.003> (2005).
43. Ghebreselassie, H. Measuring the hydrophobicity of cellulose and the effect of humidity by inverse gas chromatography. *Dissertations & Theses - Gradworks* (2013).
44. Tangsathakun, C. *et al.* The influence of molecular weight of chitosan on the physical and biological properties of collagen/chitosan scaffolds. *J Biomater Sci Polym Ed* **18**, 147–163, <https://doi.org/10.1163/15685620779116694> (2007).
45. Chen, X. *et al.* Distinction of broken cellular wall Ganoderma lucidum spores and G. lucidum spores using FTIR microspectroscopy. *Spectrochim Acta A Mol Biomol Spectrosc* **97**, 667–672, <https://doi.org/10.1016/j.saa.2012.07.046> (2012).
46. Carrasco, H. *et al.* Eugenol and its synthetic analogues inhibit cell growth of human cancer cells (part I). *Journal of the Brazilian Chemical Society* **19**, 543–548, <https://doi.org/10.1590/S0103-50532008000300024> (2008).
47. Liu, G. *et al.* In *Ico20: Biomedical Optics* Vol. 6026 *Proceedings of SPIE* (eds G. V. Bally & Q. Luo) (2006).
48. Muresan, A. E. *et al.* HPLC Determination and FT-MIR Prediction of Sugars from Juices of Different Apple Cuhivars during Fruit Development. *Notulae Botanicae Horti Agrobotanici Cluj-Napoca* **43**, 222–228 (2015).
49. Buning-Pfaue, H. Analysis of water in food by near infrared spectroscopy. *Food Chemistry* **82**, 107–115, [https://doi.org/10.1016/S0308-8146\(02\)00583-6](https://doi.org/10.1016/S0308-8146(02)00583-6) (2003).
50. Mohacek-Grosov, V., Bozac, R. & Puppels, G. J. Vibrational spectroscopic characterization of wild growing mushrooms and toadstools. *Spectrochim Acta A Mol Biomol Spectrosc* **57**, 2815–2829, [https://doi.org/10.1016/s1386-1425\(01\)00584-4](https://doi.org/10.1016/s1386-1425(01)00584-4) (2001).

51. Kozarski, M. *et al.* Antioxidative and immunomodulating activities of polysaccharide extracts of the medicinal mushrooms *Agaricus bisporus*, *Agaricus brasiliensis*, *Ganoderma lucidum* and *Pheleinus linteus*. *Food Chemistry* **129**, 1667–1675, <https://doi.org/10.1016/j.foodchem.2011.06.029> (2011).
52. Committee, N. P. Pharmacopoeia of the People's Republic of China. *Part 1*, 188–189 (2015).
53. Jiao, L., Bing, S., Zhang, X. F. & Li, H. Interval partial least squares and moving window partial least squares in determining the enantiomeric composition of tryptophan using UV-Vis spectroscopy. *Journal of the Serbian Chemical Society* **81**, 209–218, <https://doi.org/10.2298/Jsc150227065j> (2016).
54. Norgaard, L. *et al.* Interval partial least-squares regression (iPLS): A comparative chemometric study with an example from near-infrared spectroscopy. *Applied Spectroscopy* **54**, 413–419, <https://doi.org/10.1366/0003702001949500> (2000).
55. Ojamae, L., Hermansson, K. & Probst, M. The Oh Stretching Frequency in Liquid Water Simulations - the Classical Error. *Chemical Physics Letters* **191**, 500–506, [https://doi.org/10.1016/0009-2614\(92\)85416-8](https://doi.org/10.1016/0009-2614(92)85416-8) (1992).
56. Zhang, F., Huang, Q., Yan, J., Zhang, X. & Li, J. Assessment of the Effect of Trichostatin A on He La Cells through FT-IR Spectroscopy. *Analytical Chemistry* **87**, 2511–2517, <https://doi.org/10.1021/ac504691q> (2015).
57. Xue, Q., Peng, W. X. & Ohkoshi, M. Molecular bonding characteristics of Self-plasticized bamboo composites. *Pakistan Journal of Pharmaceutical Sciences* **27**, 975–982 (2014).
58. Goo, B. G. *et al.* Characterization of a renewable extracellular polysaccharide from defatted microalgae *Dunaliella tertiolecta*. *Bioresource Technology* **129**, 343–350, <https://doi.org/10.1016/j.biortech.2012.11.077> (2013).
59. Shao, L. *et al.* Partial characterization and immunostimulatory activity of exopolysaccharides from *Lactobacillus rhamnosus* KF5. *Carbohydrate Polymers* **107**, 51–56, <https://doi.org/10.1016/j.carbpol.2014.02.037> (2014).
60. Zhao, T. *et al.* Isolation, characterization and antioxidant activity of polysaccharide from *Schisandra sphenanthera*. *Carbohydrate Polymers* **105**, 26–33, <https://doi.org/10.1016/j.carbpol.2014.01.059> (2014).
61. Gruber, J. *et al.* Novel soluble blue emitting PPV-like polymers: synthesis and characterization. *E-Polymers* (2003).
62. Etcheverry, S. B., Williams, P. A. M. & Baran, E. J. Synthesis and characterization of oxovanadium(IV) complexes with saccharides. *Carbohydrate Research* **302**, 131–138, [https://doi.org/10.1016/S0008-6215\(97\)00132-8](https://doi.org/10.1016/S0008-6215(97)00132-8) (1997).
63. Petrosyan, A. M. Vibrational spectra of L-histidine perchlorate and L-histidine tetrafluoroborate. *Vibrational Spectroscopy* **43**, 284–289, <https://doi.org/10.1016/j.vibspec.2006.03.001> (2007).
64. Defrees, D. J., Miller, M. D., Talbi, D., Pauzat, F. & Ellinger, Y. The Oretical Infrared-Spectra of Some Model Polycyclic Aromatic-Hydrocarbons - Effect of Ionization. *Astrophysical Journal* **408**, 530–538, <https://doi.org/10.1086/172610> (1993).
65. Varetti, E. L. & Aymonino, P. J. Ir Spectra of Perfluoromethyl Perfluoroacetate and Perfluoromethyl Carbonate. *Journal of Molecular Structure* **7**, 155–8, [https://doi.org/10.1016/0022-2860\(71\)90016-0](https://doi.org/10.1016/0022-2860(71)90016-0) (1971).
66. Workman, J. & Weyer, L. *Practical Guide to Interpretive Near-Infrared Spectroscopy*. (CRC Press, Inc., 2007).
67. Ferreira, D. S., Poppi, R. J. & Pallone, J. A. L. Evaluation of dietary fiber of Brazilian soybean (*Glycine max*) using near-infrared spectroscopy and chemometrics. *Journal of Cereal Science* **64**, 43–47, <https://doi.org/10.1016/j.jcs.2015.04.004> (2015).
68. Fackler, K., Schwanninger, M., Gradinger, C., Hinterstoisser, B. & Messner, K. Qualitative and quantitative changes of beech wood degraded by wood-rotting basidiomycetes monitored by Fourier transform infrared spectroscopic methods and multivariate data analysis. *FEMS Microbiol Lett* **271**, 162–169, <https://doi.org/10.1111/j.1574-6968.2007.00712.x> (2007).
69. He, W. & Hu, H. Prediction of hot-water-soluble extractive, pentosan and cellulose content of various wood species using FT-NIR spectroscopy. *Bioresource Technology* **140**, 299–305, <https://doi.org/10.1016/j.biortech.2013.04.115> (2013).
70. Chen, Y. *et al.* Study on discrimination of white tea and albino tea based on near-infrared spectroscopy and chemometrics. *J Sci Food Agric* **94**, 1026–1033, <https://doi.org/10.1002/jsfa.6376> (2014).
71. Chen, J.-B., Sun, S.-Q. & Zhou, Q. Data-driven signal-resolving approaches of infrared spectra to explore the macroscopic and microscopic spatial distribution of organic and inorganic compounds in plant. *Analytical and Bioanalytical Chemistry* **407**, 5695–5706, <https://doi.org/10.1007/s00216-015-8746-7> (2015).
72. Chen, S. F., Danao, M. G., Singh, V. & Brown, P. J. Determining sucrose and glucose levels in dual-purpose sorghum stalks by Fourier transform near infrared (FT-NIR) spectroscopy. *J Sci Food Agric* **94**, 2569–2576, <https://doi.org/10.1002/jsfa.6606> (2014).

Acknowledgements

This work was supported by the National Natural Science Foundation of China (No. 11475217, No. 11775272 and No. 11635013) and the Strategic Priority Research Program of the Chinese Academy of Sciences (No. XDA08040107). We would like to thank Prof. YJ Wu group and NSRL at USTC for providing the facilities for a part of spectral measurements. We also thank Bessie Huang for proofreading the manuscript.

Author Contributions

Q.H. conceived the project and supervised the research. Y.H.M. conducted most of the experiments with assistance of H.Q.H. in preparing the samples. Q.H. and Y.H.M. analyzed the spectral data, with other co-authors J.Z.W., H.Q.H., C.Y.W. and K.C. participating in the discussion of the results. Y.H.M. and Q.H. wrote the manuscript.

Additional Information

Supplementary information accompanies this paper at <https://doi.org/10.1038/s41598-017-18422-7>.

Competing Interests: The authors declare that they have no competing interests.

Publisher's note: Springer Nature remains neutral with regard to jurisdictional claims in published maps and institutional affiliations.



Open Access This article is licensed under a Creative Commons Attribution 4.0 International License, which permits use, sharing, adaptation, distribution and reproduction in any medium or format, as long as you give appropriate credit to the original author(s) and the source, provide a link to the Creative Commons license, and indicate if changes were made. The images or other third party material in this article are included in the article's Creative Commons license, unless indicated otherwise in a credit line to the material. If material is not included in the article's Creative Commons license and your intended use is not permitted by statutory regulation or exceeds the permitted use, you will need to obtain permission directly from the copyright holder. To view a copy of this license, visit <http://creativecommons.org/licenses/by/4.0/>.

© The Author(s) 2017